Vol 88 | Issue 10 | November 2023

Water Science & Technology

ISSN 0273-1223
E-ISSN 1996-9732
iwaponline.com/wst

Water Science & Technology

Water Science & Technology Vol 88 No 10, 2633 doi: 10.2166/wst.2023.353

Effect of carboxyl and hydroxyl groups attached to the benzene ring on the photodegradation of polycyclic aromatic hydrocarbons in ice

Caihong Jiang, Shuang Xue*, Jinming Zhang, Zhaohong Zhang, Yingtan Yu and Jiyang Liu

School of Environmental Science, Liaoning University, Shenyang 110036, China
*Corresponding author. E-mail: xueshuang666@sina.com

ABSTRACT

The effect of carboxyl and hydroxyl groups attached to the benzene ring on the photodegradation of anthracene (Ant) and pyrene (Pyr) in ice was investigated. The present study aims to explore the inhibition mechanism of five dissolved organic matter (DOM) model compounds' materials such as benzoic acid, *o*-hydroxybenzoic acid, *m*-hydroxybenzoic acid, *p*-hydroxybenzoic acid, and 3-phenyl propionic acid on the degradation of Ant and Pyr in ice. The photodegradation rate of Ant and Pyr were 50.33 and 37.44% in ice, with the photodegradation rate of Ant being greater than that of Pyr. The five DOM model compounds inhibited the photolysis of Ant and Pyr, and the influence mechanism on the photodegradation of Ant and Pyr depended upon the types and positions of functional groups on the benzene. Among them, the structure in which the carboxyl group was directly connected to the benzene ring and carboxyl was located at the ortho position of a hydroxy group had a strong inhibitory effect on the photodegradation of Ant and Pyr. Light-screening effects and quenching effects were the main inhibiting mechanism, and the binding ability of DOM model compounds material and PAHs is dominantly correlated with its inhibiting effect.

Key words: dissolved organic matter, ice, light-screening effect, photodegradation, polycyclic aromatic hydrocarbons, quenching effect

HIGHLIGHTS

- Among five DOM model compounds, the structure of the carboxyl group directly connected with the benzene ring had stronger inhibition of photodegradation of Ant and Pyr.
- The inhibition of Ant and Pyr by the DOM fragment models were identified mainly due to light-screening effect and the quenching effect of DOM.

GRAPHICAL ABSTRACT

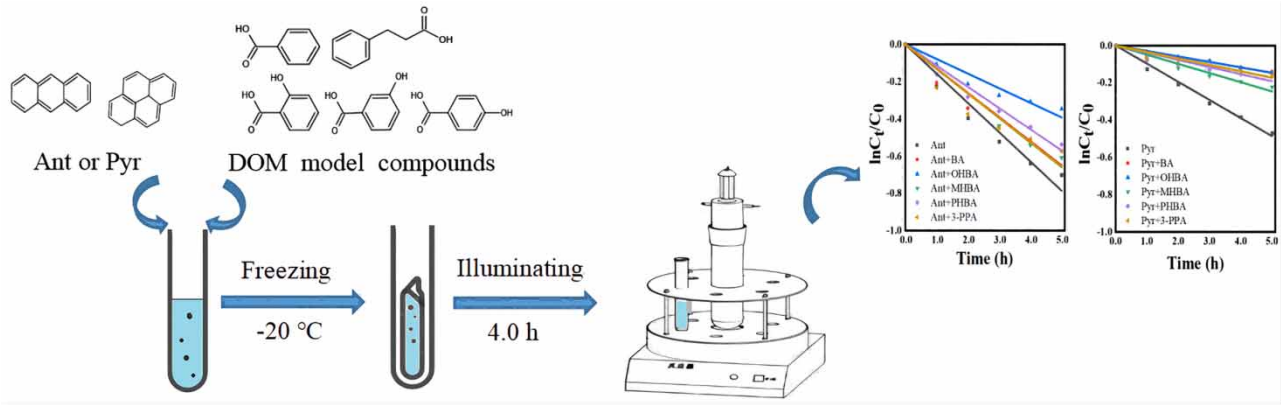

INTRODUCTION

Polycyclic aromatic hydrocarbons (PAHs) are typical volatile hydrocarbons produced by the incomplete combustion of organic compounds such as coal, oil, wood, smoke, and organic polymer compounds (Kong *et al.* 2017; Wu & Shao 2017). They are mainly compounds connected by two or more benzene rings in the form of thick rings and they show a very stable inert in the chemical reaction and continuously enrich, transfer, and transform in the environmental medium (Driskill *et al.* 2018; Liu *et al.* 2023). Due to their toxicity, mutagenicity, and carcinogenicity to human health and ecosystem, the transformation and degradation of PAHs have attracted great attention.

PAHs are ubiquitous in all environmental media, including snow, surface waters, soil, and ambient air (Ram & Anastasio 2009; Ge *et al.* 2015). The photochemical transformation is probably the main degradation process of PAHs, which plays a distinctly important role in their decomposition, transport, transformation, toxic changes, and fate (Dong *et al.* 2020). Photodegradation is especially important for the transformation of PAHs in high latitude snow packs due to low temperatures and continuous sunlit conditions. The presence of PAHs in cold regions raises critical issues for ice and snow chemistry processes (Ge *et al.* 2016b; Brogi *et al.* 2018; Hullar *et al.* 2021). Although there are similarities in the sources and light absorption properties of aquatic and ice PAHs, there are likely critical differences in the photochemical processes due to the physical properties of snow and ice (Ge *et al.* 2016a; Xue *et al.* 2019; Lin *et al.* 2022).

Previous research has identified that dissolved organic matter (DOM) plays an important role in the photodegradation of PAHs in surface waters and ice (Luo *et al.* 2022). The concentration and origin of DOM in the photodegradation of PAHs in water and ice have been reported in previous studies (Saeed *et al.* 2011; Maizel & Remucal 2017; Xue *et al.* 2019). DOM is defined as the organic materials below 0.45 μm and consists of a mixture of the decomposition products of plant and animal residues and of substances synthesized biologically and/or chemically from decomposed products or intermediate products (Chen *et al.* 2002). The chemical composition and structural characteristics of DOM can significantly influence their optical and chemical properties, photochemical reactivity, and interaction with other environmental pollutants (Chen *et al.* 2002; He & Wang 2011; Zhao *et al.* 2020). Hence, there is increasing interest in incorporating its chemical properties into the prediction of behavior of DOM and environmental pollutants in natural ecosystems. DOM is an extremely complex heterogeneous mixture with wide ranges in molecular weight and functional groups (Zularisam *et al.* 2007; Maizel & Remucal 2017; Wang *et al.* 2020). Figure 1 shows one proposed structure based on pyrolysis studies (Jones & Bryan 1998).

Since it is not practical to analyze individual components of DOM due to its heterogeneous nature, it will be more suitable to use some DOM-like model compounds, i.e., model organics with representative functional groups of DOM to investigate the correlations between DOM molecular structures and their photochemical reactivity and therefore be employed in several studies (Sun *et al.* 2015; Wang *et al.* 2020; Zhao *et al.* 2020). Wang *et al.* selected a series of phenols and other oxidated aromatic compounds containing different functional groups including hydroxyl, carboxyl, amino, methoxy, and quinones to investigate their photochemical production abilities of singlet oxygen ($^1O_2$) under simulated sunlight (Wang *et al.* 2020). Zhou *et al.* selected 17 DOM-like model compounds and a commercial DOM to construct the inherent relationships between the structure of DOM and the formation of $^1O_2$ (Zhao *et al.* 2020). In addition, He and Wang used a commercial humic acid (HA) and three aromatic acids as model HA segments to investigate the behavior of model HA segments in interacting with anthracene (Ant) (He & Wang 2011). However, to the authors' knowledge, no research has been undertaken to identify components or functional groups in DOM which are responsible for the photoproduction of reactive species and involved in the photodegradation of PAHs in ice, although such work is significant for better understanding the role of DOM in the photodegradation of PAHs.

It was identified that the HA molecules were mainly composed of aromatic moieties with carboxyl and hydroxyl substitutes, and is commonly recognized that the aromatic moieties of HS would be the main sites for the adsorption of PAHs (Gunasekara *et al.* 2003; Golding *et al.* 2005; He & Wang 2011). So, benzoic acid (BA), *o*-hydroxybenzoic acid (*o*-HBA), *m*-hydroxybenzoic acid (*m*-HBA), *p*-hydroxybenzoic acid (*p*-HBA), and 3-phenylpropionic acid (3-PPA) were selected as DOM model components in this study, which have typical aromatic rings as the main structure with conjugated carboxyl and/or hydroxyl groups at varied locations, to investigate the effect of carboxyl and hydroxyl groups attached to benzene ring as well as the position of hydroxyl groups in aromatic acids on the photodegradation of PAHs in ice. Ant with three fused benzene rings and pyrene (Pyr) with four fused benzene rings are among the most abundant PAHs in the environment and are classified as priority pollutants by the U.S. EPA (Fang *et al.* 2015), and therefore they were chosen as model pollutants in this study. The objective of this study was to explore the effect mechanisms of photodegradation of PAHs in ice caused by

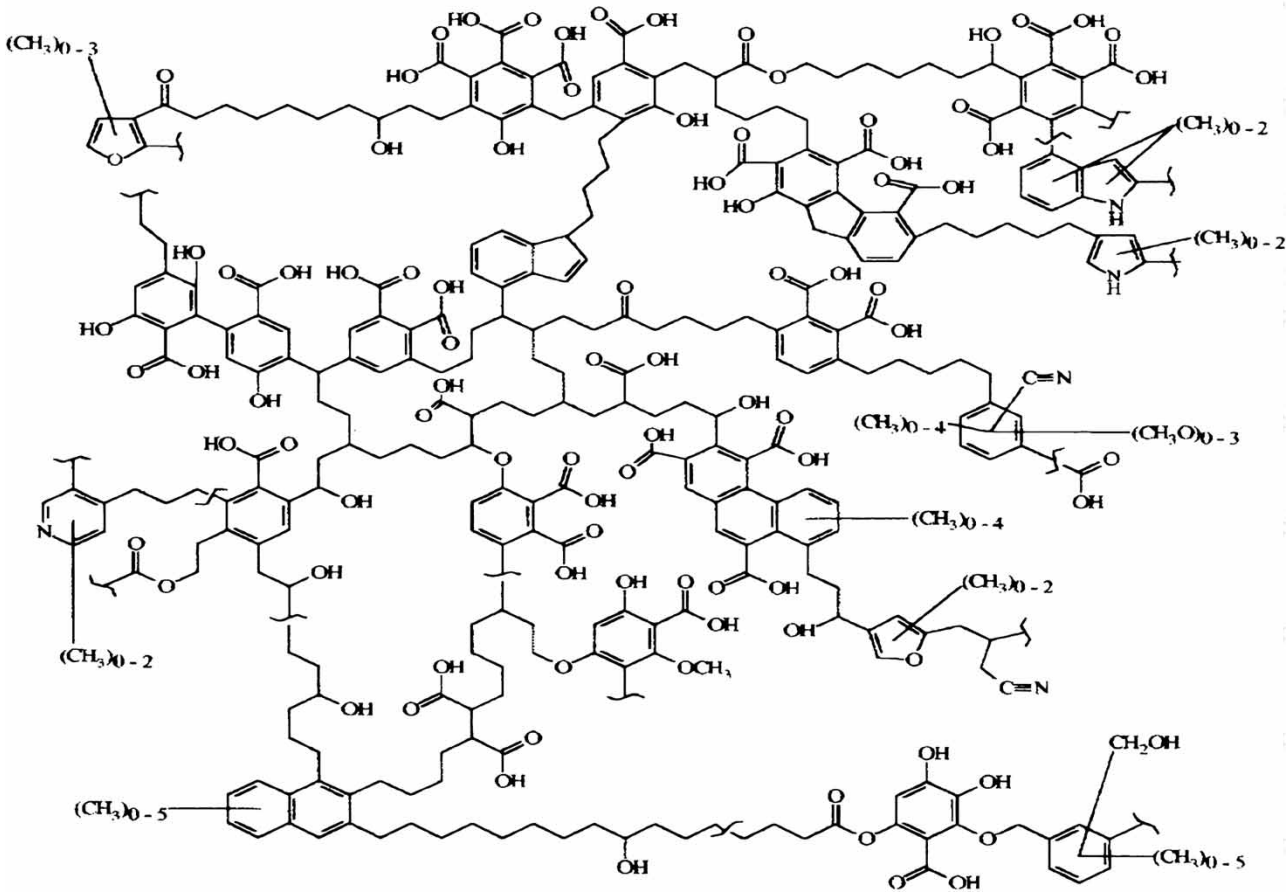

Figure 1 | State-of-the-art structural concept of DOM. Adapted from Malcolm N. Jones, Nicholas D. Bryan (Jones & Bryan 1998).

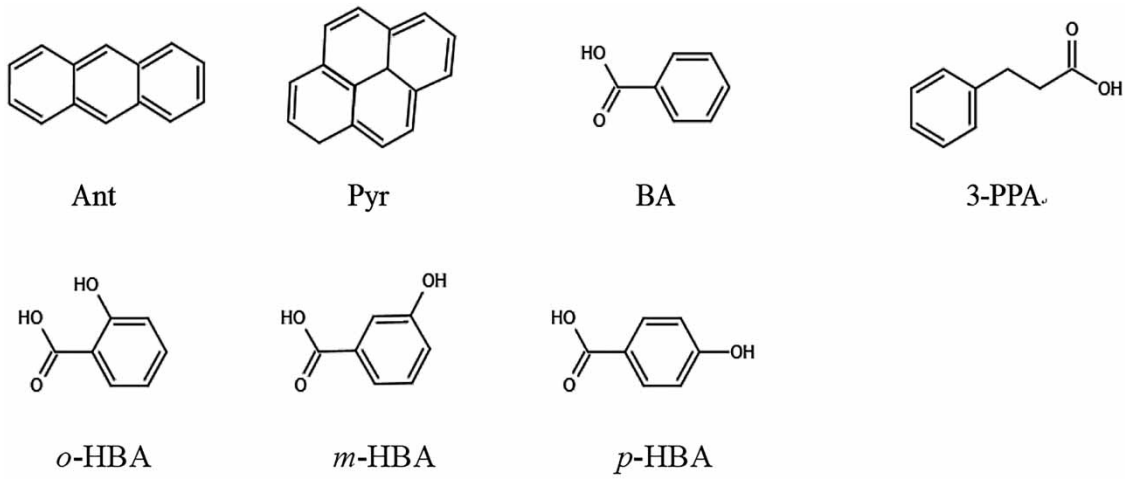

Figure 2 | Molecular structures of PAHs and DOM model compounds in this study.

five DOM model compounds. The molecular structure of PAHs and DOM model compounds also shown in Figure 2. The findings of this study may greatly improve our understanding of correlations between the structural and functional properties of DOM and their roles in the photodegradation of environmental pollutants in cold regions.

MATERIALS AND METHODS

Chemicals

Ant (99.0%), Pyr (97.0%), and *m*-HBA (98.0%) were from Shanghai McLean. *o*-HBA (99.5%) and BA (99.5%) were from Tianjin Damao Chemical Reagent Factory. 3-PPA (98.0%) was from Shanghai source leaf biology. *p*-HBA (99.0%) was from Tianjin Reagent Research Institute, and 2-nitrobenzaldehyde (2NB) was purchased from Sigma-Aldrich. High-performance liquid chromatography (HPLC) grade acetonitrile was from Fisher (USA). Deionized water was prepared with the Millipore Milli-Q system. Ant and Pyr stock solutions (200 mg L^{-1}) were prepared in acetonitrile and stored in amber borosilicate vials at 4°C in the refrigerator. DOM fragment model stock solutions (0.024 mM) were prepared in Milli-Q water and stored in amber borosilicate vials at 4°C in the refrigerator.

Sample preparation and photodegradation experiments

The illumination solution (50 μg L^{-1}) of 50 mL was pipette into Ø25 mm × 200 mm tubes, and frozen in a laboratory freezer at −20°C for photodegradation experiments. All photodegradation experiments were carried out in LY-GHX-V photochemistry reactor (Shanghai Lanyi Industrial Ltd, China). A 500 W Xenon lamp with optical filters (<290 nm) was placed in a double quartz cold trap, which was used as a sunlight simulation light source. For ice photodegradation experiments, samples were illuminated in the same way as liquid samples except that they were frozen in a freezer at −20°C before illumination. The lamp was cooled by a water jacket, and the chamber temperature was maintained at 20 ± 0.5°C and −20 ± 0.5°C for liquid and ice experiments, respectively. The illumination time was 5.0 h, and at defined intervals a duplicate set of irradiated samples were taken out and thawed at room temperature (about 25°C) in the dark for PAHs concentration determination. Dark control samples were covered with aluminum foil and placed in the illumination chamber along with illuminated samples. In order to investigate the effects of DOM model compounds on PAHs photodegradation kinetics, 50 μg L^{-1} of Ant or Pyr was added into each DOM model compounds' stock solution and subjected to photodegradation experiments. All the samples for photodegradation experiments were analyzed by ultraviolet–visible (UV–Vis) spectroscopy to investigate the interaction between DOM model compounds with PAHs.

Fluorescence measurements

Emission spectra were collected using a Cary Eclipse EL0507-3920 (Varin Company, America) spectrophotometer. The spectra were recorded at a scan rate of 1,200 nm min^{-1} using excitation and the emission slit width was 5 nm. Fluorescence was measured as a function of added DOM material at a fixed wavelength. The excitation wavelengths utilized for this study were 250 and 240 nm for Ant and Pyr, respectively. The fluorescence intensity of DOM model compounds with each concentration (i.e., total organic carbon is 1.0, 2.0, 3.0, 4.0, and 5.0 mg C L^{-1}) without PAHs present were also measured and subtracted from the total fluorescence intensity measured for PAHs in the presence of DOM model compounds before proceeding with data analysis.

Analysis

PAHs concentrations were measured with Agilent1260 HPLC equipped with a UV–Vis detector and an Agilent Zorbax SB-C18 column (5 μm particle size, 4.6 mm × 150 mm). An eluent of 90:10 (v/v) acetonitrile: MQ water was used at a flow rate of 1.40 mL min^{-1} and the column temperature was controlled at 25°C. The detection wavelengths were 251 and 240 nm for Ant and Pyr, respectively.

UV/Vis spectra were analyzed using a Cary-50 ultraviolet–visible spectrophotometer (Varian Company, USA).

RESULTS AND DISCUSSION

Photolysis kinetics of Ant and Pyr in ice

Studies with 50 μg L^{-1} Ant and Pyr in ice and water samples with 5 h irradiation were carried out to investigate the direct photochemical degradation of Ant and Pyr. The photolysis kinetics was described with quasi-primary reaction dynamics, and the apparent photolysis rate (k) as well as photolysis half-life time ($t_{1/2}$) were determined from the following equation

(Kang *et al.* 2009; Ram & Anastasio 2009; Fan *et al.* 2022):

$$\ln \frac{C_t}{C_0} = -k \cdot t \tag{1}$$

$$t_{1/2} = \frac{\ln^2}{k} = \frac{0.693}{k} \tag{2}$$

where t is the photolysis time, C_0 and C_t are the PAH concentrations at time zero and t, respectively. The photodegradation kinetic parameters of PAHs in five DOM model compounds were compared.

As shown in Figure 3, the photodegradation of Ant and Pyr could be fit with first-order kinetics in both water and ice. The reaction rate constants for Ant and Pyr were 0.174 (0.96) and 0.092 (0.97) in water, and 0.157 (0.97) and 0.097 (0.99) in ice, respectively, and the values in parentheses represent the correlation coefficient (r) of the linear regression of concentration over time. The half-life time of Ant and Pyr were 3.98 and 7.53 h in water, and 4.41 and 7.12 h in ice, respectively. It is noteworthy that the photodegradation rate of Ant in water was approximately 37% higher than that of Pyr, and 26% higher in ice

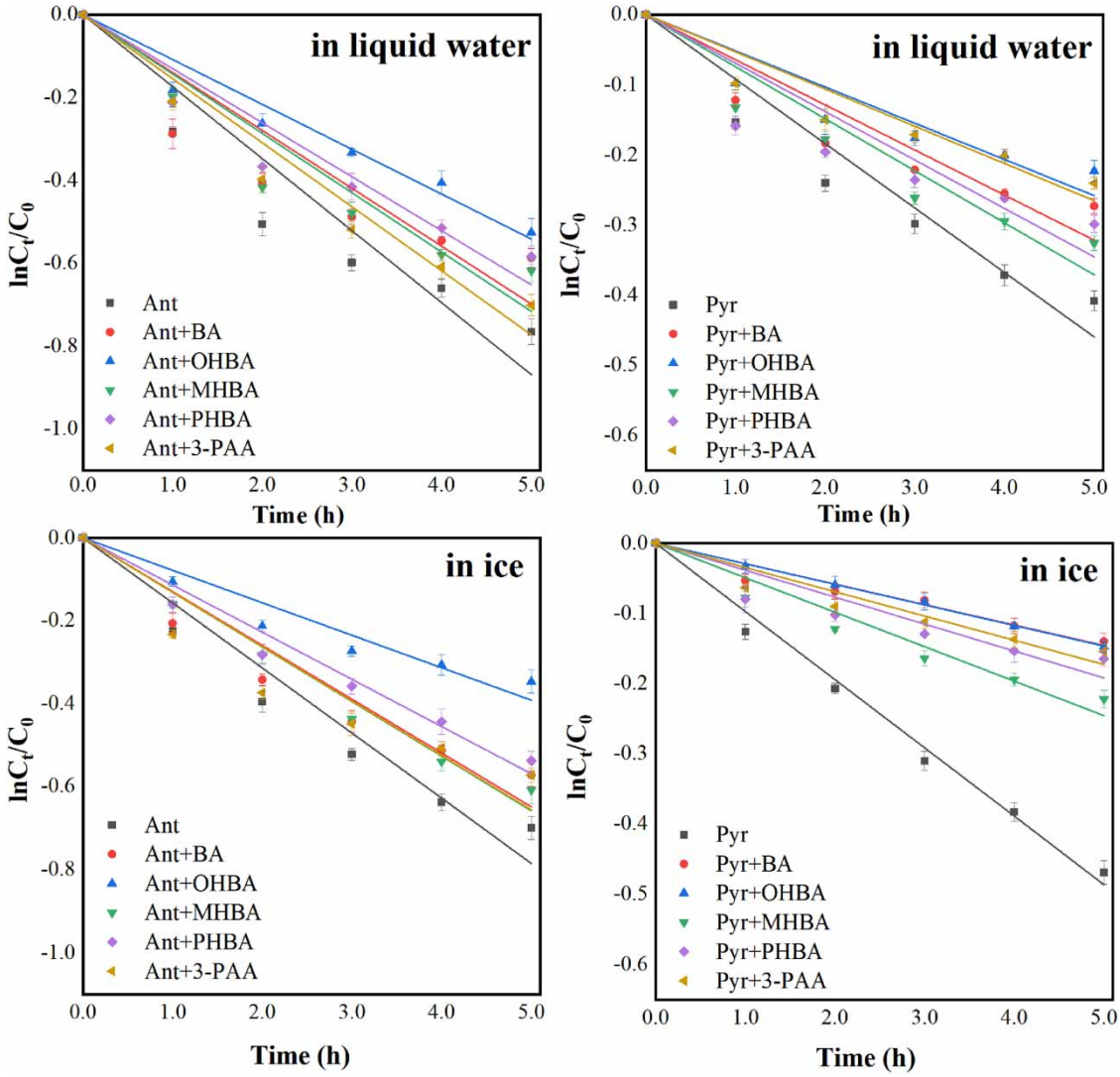

Figure 3 | Photodegradation of Ant and Pyr with and without DOM model compounds present in ice.

compared to Pyr. The difference in photolysis rates between Ant and Pyr may be attributed to variations in their molecular structures and photodegradation mechanisms. Among them, the k range of photodegradation of Ant and Pyr in five DOM model compounds were 0.078–0.132 and 0.029–0.049 h^{-1} (Table 1), respectively, which were smaller than their own photolysis in ice. Obviously, all five DOM fragment compounds exhibited suppressing effects on Ant and Pyr photodegradation kinetics in ice, nevertheless, the degree of inhibition varied distinctively depending on the structure of the DOM fragment compounds. For instance, the order of k value of Ant and Pyr with DOM fragment compounds were 3-PPA (0.131 h^{-1}) > BA (0.130 h^{-1}) and 3-PPA (0.035 h^{-1}) > BA (0.029 h^{-1}) in ice, respectively. Thus, BA had a stronger inhibitory effect on the photodegradation of Ant and Pyr compared with BA and 3-PPA, which indicated that the carboxyl directly connected to the benzene ring had a stronger effect on the photodegradation of Ant and Pyr. Meanwhile, the photodegradation rates of Ant and Pyr with *o*-HBA present were 40.88 and 19.97%, respectively, which were lower than those with other DOM model compounds present. Therefore, when a carboxyl was located at the ortho position of a hydroxy group, significant inhibition of the photodegradation of Ant and Pyr was observed.

Previous research has shown that the number of photons received in ice differs from that in liquid water. The 2-nitrobenzaldehy (2NB) is a convenient, robust chemical actinometer, with fast time resolution and straightforward photochemistry. Therefore, the local photon flux was measured in liquid water and ice samples by chemical actinometry using 2NB (Malley *et al.* 2017). Identical volumes of 2NB samples (10 μM) were prepared using the same freezing method. Then liquid water and ice samples were illuminated for 60 min in the same illumination system as for PAHs samples. 2NB concentrations were analyzed by using the same HPLC as for the PAHs analyses, with an eluent of 60:40 acetonitrile: MQ water and a wavelength of 226 nm. 2NB photolysis kinetics in liquid water and ice are shown in Figure 4. The photon fluxes (I_λ) in liquid and ice samples can be expressed as

$$I_\lambda = \frac{j(\mathrm{2NB})}{2.303 \times \varepsilon_{\mathrm{2NB},\lambda} \emptyset_{\mathrm{2NB},\lambda} \times l} \tag{3}$$

where j(2NB) is the optical loss rate constant of 2NB, $\varepsilon_{2\mathrm{NB},\lambda}$ is the molar absorption coefficient of 2NB at the λ wavelength, and $\Phi_{2\mathrm{NB},\lambda}$ is the product of the molar absorptivity and quantum efficiency of 2NB with a value of 0.41, l is the cell path length (cm) (Sharpless 2012). In this study, it was observed that photon fluxes in ice were approximately 14.3% lower than in liquid water. This difference can partially explain the faster photolysis of anthracene and pyrene in water compared to ice.

Table 1 | Kinetics parameter of the influence of DOM model compounds on the photolysis of Ant and Pyr in ice

Samples	K_{obs} (h^{-1})[a]	K_{DOM}	S_λ[b]	S_λ'	S_λ'/S_λ	Q_λ
Ant						
BA	0.017 ± 0.002	0.130 ± 0.009	0.9378	0.1104	0.1177	0.8823
o-HBA	0.052 ± 0.007	0.078 ± 0.005	0.8283	0.3296	0.3979	0.6021
m-HBA	0.008 ± 0.010	0.132 ± 0.006	0.8929	0.0540	0.0605	0.9395
p-HBA	0.041 ± 0.019	0.114 ± 0.005	0.9867	0.2612	0.2647	0.7353
3-PPA	0.0120 ± 0.010	0.131 ± 0.011	0.9608	0.1245	0.1296	0.8704
Pyr						
BA	0.062 ± 0.001	0.029 ± 0.002	0.9310	0.6340	0.6809	0.3190
o-HBA	0.051 ± 0.007	0.029 ± 0.001	0.8227	0.5216	0.6340	0.3660
m-HBA	0.037 ± 0.008	0.049 ± 0.003	0.8868	0.3811	0.4298	0.5702
p-HBA	0.057 ± 0.001	0.038 ± 0.003	0.9794	0.5847	0.5970	0.4030
3-PPA	0.058 ± 0.006	0.035 ± 0.003	0.9538	0.5982	0.6272	0.3728

[a]The observed rate constant of Ant and Pyr photodegradation in the presence of DOM model compounds.
[b]The light-screening factor was calculated for wavelengths.

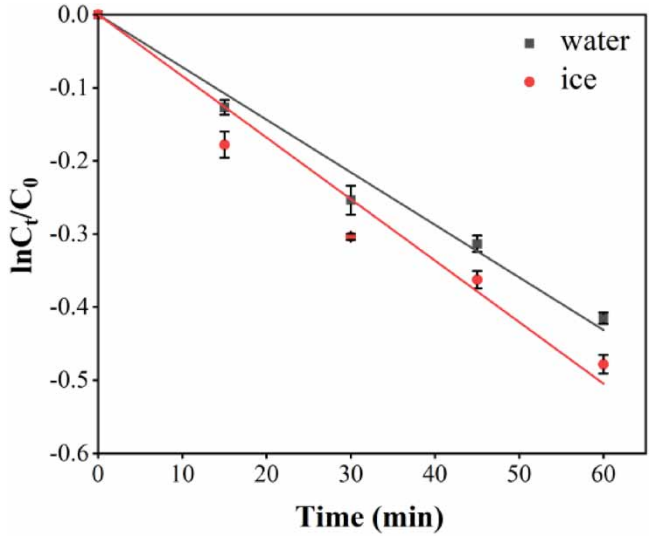

Figure 4 | 2NB photodegradation in liquid water and ice ([2NB] = 10 μM).

It is important to note that the effects of lens refraction were already accounted for in the measured photon flux determined by actinometry. This issue was addressed using Snell's law and calculated from Equations (4) and (5) for length l (Sharpless 2012):

$$\eta_w \sin\theta_t = \eta_a \sin\theta_i \tag{4}$$

$$l = 2r\cos\left[\sin^{-1}(\sin\theta_i(\eta_a/\eta_w))\right] \tag{5}$$

where η_w and η_a are there fractive indices of water and air, respectively. The r is the glass tube diameter (2.5 cm), θ is between 0° and 90° and calculating the average.

The resulting average path length was determined to be 1.475 cm in water and 1.679 cm in ice. Consequently, the optical diameter length in ice was approximately 13.8% greater than in water, which would lead to increased optical shielding. Furthermore, the presence of a quasi-liquid layer in ice resulted in higher local concentration in frozen samples, indicating that the environmental medium has a significant impact on these effects.

Inhibition effect of DOM model compounds on the photodegradation of PAHs light-screening effects analysis

It is generally believed that the inhibition of photolysis of PAHs by DOM is mainly due to its light-screening effects and quenching effects (Xia *et al.* 2009). The action size of the light-screening effects can be represented by calculating quenching effect of the theoretical value (S_λ) expressed by Equation (6):

$$S_\lambda = \frac{1 - 10^{-(-\alpha_\lambda + \varepsilon_\lambda C_{\mathrm{PAHs}})l}}{2.303(-\alpha_\lambda + \varepsilon_\lambda C_{\mathrm{PAHs}})l} \tag{6}$$

where α_λ (cm^{-1}) is the wavelength-specific attenuation coefficient, ε_λ ($\mathrm{M}^{-1}\,\mathrm{cm}^{-1}$) represents the molar absorptivity of PAHs, C_{PAHs} (mol L^{-1}) is concentrations of PAHs, and l (cm) is the optical path length (1.679 cm) (Sharpless 2012). If this light-screening effect is considered, the observed degradation rate constant (k_{obs}) can be calculated with the following equation:

$$k_{\mathrm{obs}} = k_d \cdot S_\lambda - k_{\mathrm{DOM}} \tag{7}$$

where the k_{d} is the direct degradation rate constant for Ant and Pyr alone and the k_{DOM} is the rate constant caused by the quenching effect of DOM model compounds.

Walse *et al.* proposed that the quenching effect of DOM can be estimated by the quenching factor Q_λ, with the formula shown in Equation (8) (Gauthier *et al.* 1987; Zeng *et al.* 2012; Tang *et al.* 2020):

$$Q_\lambda = 1 - \frac{S'_\lambda}{S_\lambda} \tag{8}$$

$$S'_\lambda = \frac{K_{\text{obs}}}{k_d} \tag{9}$$

Table 1 shows that the ratio of actual value to the theoretical value of five DOM model compounds is all less than 1 (i.e., $S_\lambda'/S_\lambda < 1$), indicating that the photolysis rate of Ant and Pyr was inhibited or quenched to a greater extent that would be predicted from light attenuation by DOM model compounds alone. The S_λ values of the *o*-HBA were 0.828 and 0.823 in Ant and Pyr, which were significantly lower than those for the other four DOM model compounds. The S_λ value indicated that the light-screening effect of DOM model compounds, which further affected the light absorption of Ant and Pyr (Zhang *et al.* 2022). Thus, *o*-HBA had a stronger screening effect compared to the other four DOM model compounds, suggesting that the photodegradation of Ant and Pyr was further inhibited. Additionally, Q_λ value for *o*-HBA was significantly higher than those for the other four DOM model compounds. The results suggested that the quenching effect of *o*-HBA on the photodegradation rate of Ant and Pyr in ice was not weak, or in other words, the higher observed inhibition effect of *o*-HBA on Ant and Pyr photodegradation might be ascribed to its higher quenching effect. Previous studies reported that the quenching effect was mainly related to the binding ability of DOM and organic pollutants (Walse *et al.* 2004). The effect of binding capacity on the photolysis of PAHs will be analyzed in detail in the next section.

Analysis of the binding ability of DOM model compounds with Ant and Pyr

The fluorescence quenching technique is derived from the observation that the intensity of fluorescence is proportionately decreased upon the addition of DOM model compounds.

The correlation of PAHs with DOM model compounds may be represented by the following equations:

$$\text{PAHs (aq)} + \text{DOM (aq)} \rightarrow \text{PAHs} - \text{DOM (aq)} \tag{10}$$

$$K_{\text{doc}} = \frac{[\text{PAHs} - \text{DOM}]}{[\text{PAHs}][\text{DOM}]} \tag{11}$$

where DOM is DOM model compounds, PAHs-DOM is DOM model compounds polycyclic aromatic hydrocarbons, and K_{doc} is the partition coefficients of PAHs between DOM model compounds.

The mass balance of PAHs is described in Equation (12), where $[\text{PAHs}]_0$ is the total concentration of PAHs.

$$[\text{PAHs}]_0 = [\text{PAHs}] + [\text{PAHs} - \text{DOM}] \tag{12}$$

In theory, the intensity is proportional to the concentration of PAHs, then

$$\frac{F_0}{f} = 1 + k_{\text{dom}}[\text{DOM}] \tag{13}$$

where F_0 and f represent fluorescence intensity in the existence and deficiency of the DOM fragment model, severally. Equation (13) is in the form of the Stern–Volmer equation.

Figure 5 displays the Stern–Volmer plots of the DOM model compounds binding to Ant and Pyr. The fluorescence intensity of PAHs varied with the concentration gradient of the added DOM fragment model, confirming that DOM model compounds bind to PAHs (Schlautman & Morgan 1993; Mei *et al.* 2009).

Table 2 displays the values of $\log K_{\text{doc}}$ and K_{doc} for the two PAHs binding to the five DOM model compounds. The binding ability of the DOM fragment model for both Ant and Pyr was in turn: *p*-HBA > BA > *m*-HBA > *o*-HBA > 3-PPA. In this study, the values of $\log K_{\text{doc}}$ displayed in the range of 3.60–5.34 and 3.15–5.52 for Ant and Pyr, respectively. The binding capacity of DOM model compounds and Pyr was slightly stronger than Ant, indicating that the higher hydrophobicity of

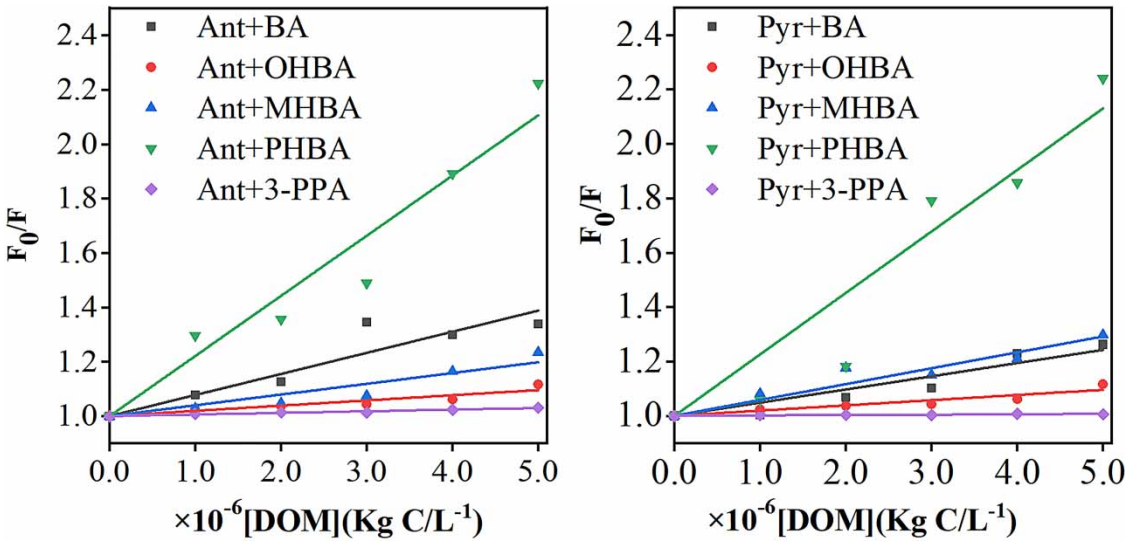

Figure 5 | Stern–Volmer plots of five DOM model compounds in ice.

Table 2 | Binding constants of Ant and Pyr with DOM model compounds in ice

	Ant		Pyr	
DOM model compounds	K_{doc} (L·kg^{-1})	LogK_{doc}	K_{doc} (L·kg^{-1})	LogK_{doc}
BA	7.75×10^4	4.889	8.05×10^4	4.906
o-HBA	1.92×10^4	4.283	7.56×10^4	4.879
m-HBA	3.96×10^4	4.597	7.96×10^4	4.901
p-HBA	2.21×10^5	5.344	3.32×10^5	5.521
3-PPA	5.90×10^3	3.770	6.60×10^3	3.820

Pyr. Perminova also observed that pyrene K_{doc} values are a factor of 2–10 higher than for Ant (Perminova *et al.* 1999). Compared with BA, *o*-HBA, *m*-HBA, 3-PPA, the binding ability between *p*-HBA and PAHs is the strongest, which had a strong electron absorption carboxyl group in the benzene ring. The ends of the conjugate system connected to the electron group and electron absorption group type D-π-A molecules to generate polymer in the solution, which had a larger surface area to enhance its effect with PAHs (Zhu *et al.* 2004; Kulhánek *et al.* 2021). Therefore, *p*-HBA had the strongest binding ability to PAHs. It was found that reagents with *p*-substituted DOM fragment compounds give stronger binding ability with PAHs than those with *o*-substituted or *m*-substituted groups. 3-PPA was aromatic carboxylic acids with aromatic ring side chains that are directly connected to adipose carbon, which is far less related to PAHs than aromatic carboxylic acids directly linked to the benzene ring. The binding effect of the two may be only caused by molecular hydrophobic force (Perminova *et al.* 1999; Mei *et al.* 2009). For the binding ability of the DOM model compounds with PAHs, *p*-HBA showed the strongest binding ability with PAHs and its binding constant two orders of magnitude was larger than that of 3-PPA. Therefore, the structure with the carboxyl group directly attached to the benzene ring may play an important role in the bonding interaction between DOM and PAHs. Meanwhile, the position of the hydroxyl on the benzene ring may change the strength of the π–π interaction between DOM and PAHs, which in turn affects their bonding ability.

UV–Vis spectrum analysis

The UV spectra are used for studying the interaction between DOM model compounds with PAHs as displayed in Figure 6(a). The absorption peak of Ant itself appeared at 252 nm and Pyr appeared at 242 and 273 nm (Figure 6(a)), which were assigned to π–π transition of a conjugated system (He *et al.* 2019). After 5 h of illumination, the absorbance of Ant and Pyr at the

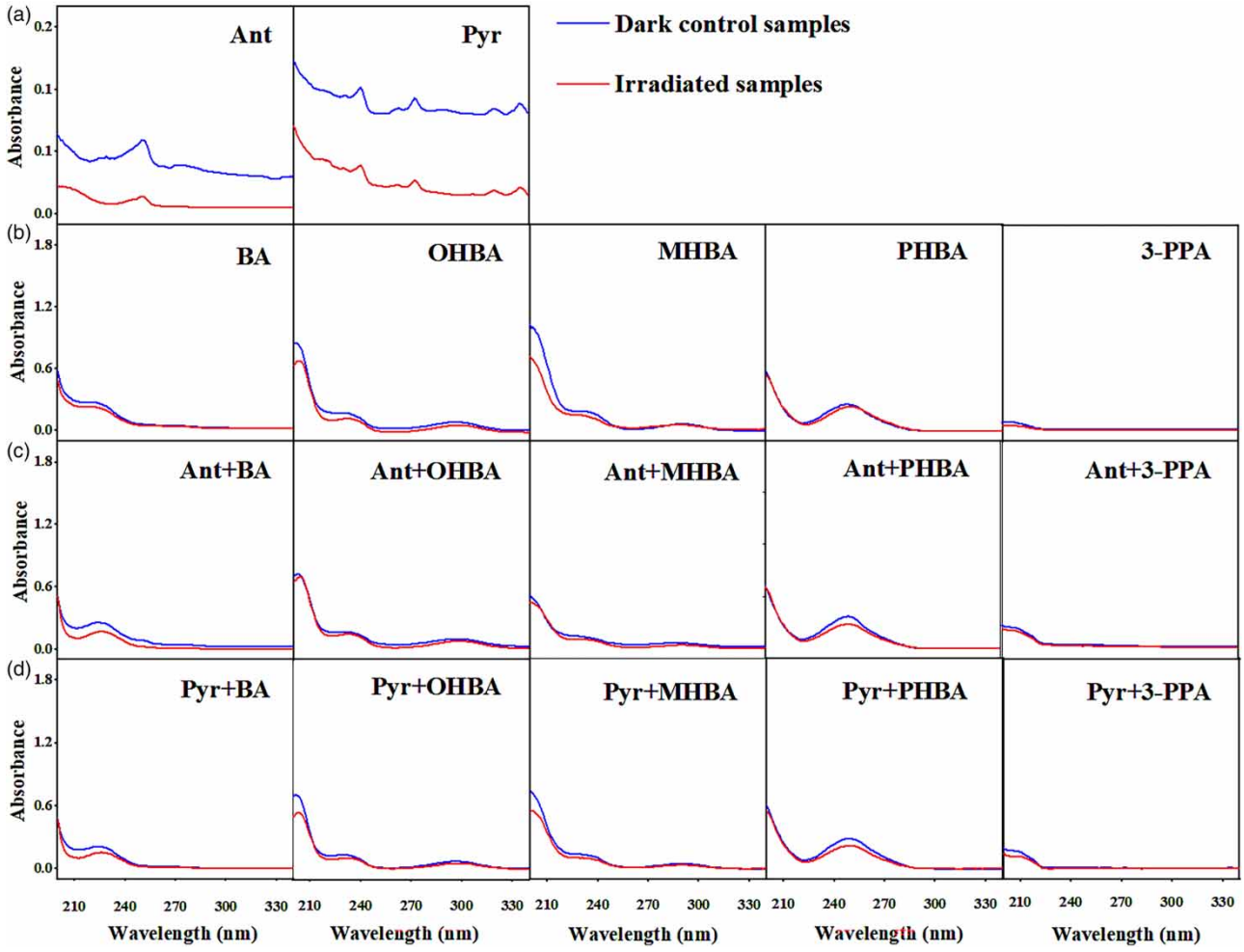

Figure 6 | (a) Photolysis UV spectra of anthracene and pyrene. (b) Photolysis UV of DOM fragment models. (c) Photolysis UV spectra of mixtures of DOM fragment models and anthracene. (d) Photolysis UV spectra of DOM fragment models and pyrene.

maximum UV absorption peak decreased significantly, the shoulder peak weakened at 242 and 273 nm of pyrene, and other characteristic peaks weakened to varying degrees, which indicated that illumination had a great influence on anthracene and pyrene. Meanwhile, Pyr had strong light absorption between 200 and 340 nm than Ant. Keren Ram *et al*. in their research demonstrated that fluoranthene (Flu) and Pyr with strong absorbance in the sunlight spectrum were more affected by photodegradation (Ram & Anastasio 2009). As shown in Figure 6(b), five kinds of DOM have light absorption in the wavelength range of 200–300 nm. The absorbance of DOM decreased in different degrees after 5 h of illumination, and the position of the UV absorption peak changed. The UV spectra of BA showed a strong absorption band around 231 nm in ice, and it was assigned to the π–π transition of the CT ring. The UV spectra of *o*-HBA, *m*-HBA, and *p*-HBA showed strong absorption bands of 235, 237, and 246 nm, respectively. After 5 h of illumination, the strong absorption band of *o*-HBA, *m*-HBA, and *p*-HBA were changed to 238, 240, and 251 nm, respectively. The position of the characteristic peak had a certain degree of the red-shift phenomenon, which was produced by the auxochrome with hydroxy aromatic structures reducing the transition energy of π–π, and the absorption wavelength of the chromophore moved towards the long wavelength (Wijnja *et al.* 2004). According to Figure 6(c) and 6(d), the absorbance of Ant and Pyr at the characteristic peak was significantly reduced when PAHs and DOM model compounds were mixed; indeed: DOM model compounds competed with Ant and Pyr for sunlight energy. Moreover, the PAHs were easy to be polarized and served as electron donors, the carboxyl protons and the electron-absorbing aromatic ring of DOM model compounds were attractive to the electron-rich large bonds of PAHs, and the π-donor solutes in Ant and Pyr interacted with π-acceptor sites in the DOM fragment model with carboxyl group (Korshin *et al.* 1997; Vecchio & Blough 2004; Kulhánek *et al.* 2021).

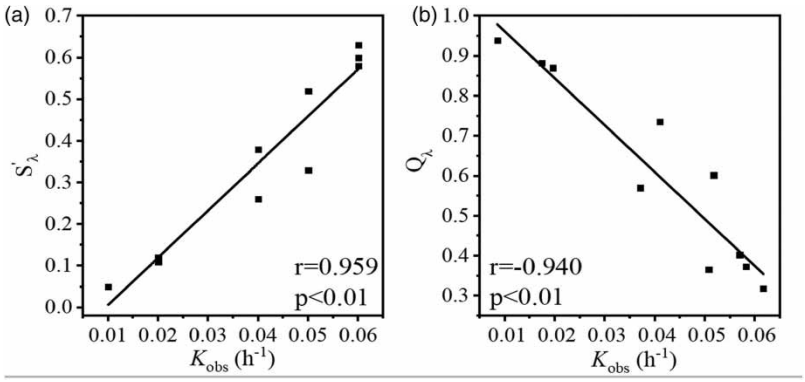

Figure 7 | Correlations between (a) K_{obs} and S_λ', and (b) K_{obs} and Q_λ.

Correlations between the photodegradation of PAHs in the presence of DOM model compounds in ice with S_λ' and Q_λ

As illustrated in Figure 7, the K_{obs} of Ant and Pyr degradation were significantly correlated with S_λ' and Q_λ of the DOM fragment model ($p < 0.01$). Similarly, as shown in Figure 7(a), a quite good positive correlation ($r = 0.959$, $p < 0.01$) was observed when examining the relationship between K_{obs} and S_λ', which proved that their inhibition effect on Ant and Pyr photodegradation was positively correlated with the optical shielding effect of DOM model compounds. The stronger the light screening was, the stronger the inhibition was. Some researchers suggested that the binding of PAHs to DOM could inhibit excited-state PAHs formation and thus, reduce the photodegradation rate constants of PAHs. In this study, it was also found that Q_λ well negatively correlated with K_{obs} ($r = -0.940$, $p < 0.01$) (Figure 7(b)), suggesting that the inhibition effect on Ant and Pyr photodegradation was strongly related to the quenching effect of DOM model compounds.

CONCLUSIONS

This work studied the effect of carboxyl and hydroxyl groups attached to the benzene ring on the photodegradation of Ant and Pyr in ice. On the basis of the experimental results, the key findings were summarized:

(1) In the presence of the DOM model compounds, the photodegradation rates of Ant and Pyr in ice were reduced by 17–50% and 50–70%, respectively.
(2) Among five DOM model compounds, the structure of a carboxyl was located at the ortho position of a hydroxy group (i.e., *o*-HBA) was favorable for the inhibition of the photodegradation of Ant and Pyr.
(3) Compared BA with 3-PAA, the structure of the carboxyl group directed connection with the benzene ring (i.e., BA) had stronger inhibition of photodegradation of Ant and Pyr.
(4) For five DOM model compounds, the K_{obs} of Ant and Pyr were well correlated with S_λ' and Q_λ ($p < 0.01$). Therefore, the inhibition effect of Ant and Pyr by the DOM model compounds was mainly due to the light-screening effect and quenching effect of DOM.

ENVIRONMENTAL SIGNIFICANCE

Ice is an important medium in the cryosphere that has the potential to influence the environmental behavior and fate of pollutants that can be transported over long distances. Compared with the perennially frozen waters of alpine and polar regions, seasonally frozen waters are heavily influenced by human activities. The role of DOM photochemistry, is known to be an important chromophore in snow and ice, and therefore it is environmentally important to discuss the effects of DOM on photodegradation of organic pollutants in ice environments. In addition, when waters receiving PAHs freeze, anthracene (Ant), pyrene (Pyr), and DOM can exist in ice. Their environmental fate could be greatly influenced by the chemical reactions occurring in ice. Here, we found that in the presence of the DOM model compounds, the photodegradation rates of Ant and Pyr in ice were reduced. Furthermore, the structure of a carboxyl was located at the ortho position of a hydroxy group (i.e., *o*-HBA) was favorable for the inhibition of the photodegradation of Ant and Pyr.

ACKNOWLEDGEMENTS

The work was supported by the Open Subject Project of Key Laboratory of Water Environment in Songliao Basin, Ministry of Education.

DATA AVAILABILITY STATEMENT

All relevant data are included in the paper or its Supplementary Information.

CONFLICT OF INTEREST

The authors declare there is no conflict.

REFERENCES

Brogi, S. R., Ha, S. Y., Kim, K., Derrien, M., Yun, K. L. & Jin, H. 2018 Optical and molecular characterization of dissolved organic matter (DOM) in the Arctic ice core and the underlying seawater (Cambridge Bay, Canada): Implication for increased autochthonous DOM during ice melting. *Sci. Total Environ.* **627**, 802–811.

Chen, J., Gu, B., Leboeuf, E. J., Pan, H. & Dai, S. J. 2002 Spectroscopic characterization of the structural and functional properties of natural organic matter fractions. *Chemosphere* **48** (1), 59–68.

Dong, Y., Peng, W., Liu, Y. & Wang, Z. 2020 Photochemical origin of reactive radicals and halogenated organic substances in natural waters: A review. *J. Hazard. Mater.* **401**, 123884.

Driskill, A. K., Alvey, J., Dotson, A. D. & Tomco, P. L. 2018 Monitoring polycyclic aromatic hydrocarbon (PAH) attenuation in Arctic waters using fluorescence spectroscopy. *Cold Reg. Sci. Technol.* **145**, 76–85.

Fan, J., Sun, X., Liu, Y., Zhao, D., Hao, X., Liu, W. & Cai, Z. 2022 New insight into environmental photochemistry of PAHs induced by dissolved organic matters: A model of naphthalene in seawater. *Process Saf. Environ. Prot.* **161**, 325–333.

Fang, Y., John, G. F., Hayworth, J. S. & Clement, T. P. 2015 Long-term monitoring data to describe the fate of polycyclic aromatic hydrocarbons in deepwater horizon oil submerged off Alabama's beaches. *Sci. Total Environ.* **508**, 46–56.

Gauthier, T. D., Seitz, W. R. & Grant, C. L. 1987 Effects of structural and compositional variations of dissolved humic materials on pyrene KOC values. *Environ. Sci. Technol.* **21** (3), 243–248.

Ge, L. K., Ren, H. L., Huo, C., Na, G. S., Wang, Y., Li, K., Zhang, P. & Jiang, H. 2015 Photochemical degradation of 9-hydroxyfluorene in ices. *Sci. China-Chem.* **45** (6), 655–661.

Ge, L. K., Li, J., Na, G. S., Chen, C. E., Huo, C., Zhang, P. & Yao, Z. W. 2016a Photochemical degradation of hydroxy PAHs in ice: Implications for the polar areas. *Chemosphere* **155**, 375–379.

Ge, L. K., Na, G. S., Chen, C. E., Li, J., Ju, M. W., Wang, Y., Li, K., Zhang, P. & Yao, Z. W. 2016b Aqueous photochemical degradation of hydroxylated PAHs: Kinetics, pathways, and multivariate effects of main water constituents. *Sci. Total Environ.* **547**, 166–172.

Golding, C. J., Birch, G. F. & Smernik, R. J. 2005 Investigation of the role of structural domains identified in sedimentary organic matter in the sorption of hydrophobic organic compounds. *Environ. Sci. Technol.* **39** (11), 3925–3932.

Gunasekara, A. S., Simpson, M. I. & Xing, B. J. 2003 Identification and characterization of sorption domains in soil organic matter using structurally modified humic acids. *Environ. Sci. Technol.* **37** (5), 852–858.

He, Y. Y. & Wang, X. C. 2011 Adsorption of a typical polycyclic aromatic hydrocarbon by humic substances in water and the effect of coexisting metal ions. *Colloids Surf. A* **379** (1–3), 93–101.

He, Y. Y., Wang, X. C., Jin, P. K., Zhao, B. & Fan, X. 2019 Complexation of anthracene with folic acid studied by FTIR and UV spectroscopies. *Spectrochim. Acta Part A* **72** (4), 876–879.

Hullar, T., Tran, T., Chen, Z., Bononi, F., Palmer, O. & Donadio, D. 2021 Enhanced photodegradation of dimethoxybenzene isomers in/on ice compared to in aqueous solution. *Copernicus GmbH* **22**, 5943–5959.

Jones, M. N. & Bryan, N. D. 1998 Colloidal properties of humic substances. *Adv. Colloid Interface Sci.* **78** (1), 1–48.

Kang, C. L., Gao, H. J., Guo, P., Zhang, G. S., Tang, X. J. & Peng, F. 2009 Kinetics and mechanism of para-chlorophenol photoconversion with the presence of nitrite in ice. *J. Hazard. Mater.* **170** (1), 163–168.

Kong, L., Gao, Y., Zhou, Q., Zhao, X. & Sun, Z. 2017 Biochar accelerates PAHs biodegradation in petroleum-polluted soil by biostimulation strategy. *J. Hazard. Mater.* **343**, 276–284.

Korshin, G. V., Li, C. W. & Benjamin, M. M. 1997 Monitoring the properties of natural organic matter through UV spectroscopy: A consistent theory. *Water Res.* **31** (7), 1787–1795.

Kulhánek, J., Pytela, O., Bure, F. & Klikar, M. 2021 Small heterocyclic D-π-D-π-A push-pull molecules with complex electron donors. *Eur. J. Org. Chem.* **22**, 3223–3233.

Lin, Y., Cai, M., Chen, M., Huang, P., Lei, R. & Chen, M. 2022 Evidence for the growing importance of Eurasian local source to PAHs in the Arctic central basin. *Sci. Total Environ.* **851** (2), 158373.

Liu, Z., Sun, X., Fu, J., Liu, W. & Cai, Z. 2023 Elevated nitrate promoted photodegradation of PAHs in aqueous phase: Implications for the increased nutrient discharge. *J. Hazard. Mater.* **443**, 130143.

Luo, H., Cheng, Q., He, D., Wang, X. & Pan, X. 2022 Effects of photoirradiation on mercury binding to dissolved organic matter: Insights from FT-IR and synchronous fluorescence two-dimensional correlation spectroscopy. *Chemosphere* **287**, 132027.

Maizel, A. C. & Remucal, C. K. 2017 Molecular composition and photochemical reactivity of size-fractionated dissolved organic matter. *Environ. Sci. Technol.* **51** (4), 2113–2123.

Malley, P. P. A., Grossman, J. N. & Kahan, T. F. 2017 Effects of chromophoric dissolved organic matter on anthracene photolysis kinetics in aqueous solution and ice. *J. Phys. Chem. A* **121**, 7619–7626.

Mei, Y., Wang, F. C., Wang, L. Y., Bai, Y. C., Li, W. & Liao, H. Q. 2009 Binding characteristics of perylene, phenanthrene and anthracene to different DOM fractions from lake water. *J. Environ. Sci*. **21**, 414–423.

Perminova, I. V., Grechishcheva, N. Y. & Petrosyan, V. S. 1999 Relationships between structure and binding affinity of humic substances for polycyclic aromatic hydrocarbons: Relevance of molecular descriptors. *Environ. Sci. Technol.* **33** (21), 3781–3787.

Ram, K. & Anastasio, C. J. 2009 Photochemistry of phenanthrene, pyrene, and fluoranthene in ice and snow. *Atmos. Environ.* **43** (14), 2252–2259.

Saeed, T., Ali, L. N., Al-Bloushi, A., Al-Hashash, H. & Al-Khayat, A. J. 2011 Effect of environmental factors on photodegradation of polycyclic aromatic hydrocarbons (PAHs) in the water-soluble fraction of Kuwait crude Oil in seawater. *Mar. Environ. Res.* **72** (3), 143–150.

Schlautman, M. A. & Morgan, J. J. 1993 Effects of aqueous chemistry on the binding of polycyclic aromatic hydrocarbons by dissolved humic materials. *Environ. Sci. Technol.* **28** (2), 366.

Sharpless, C. M. 2012 Lifetimes of triplet dissolved natural organic matter (DOM) and the effect of $NaBH_4$ reduction on singlet oxygen quantum yields: Implications for DOM photophysics. *Environ. Sci. Technol.* **46** (8), 4466–4473.

Sun, L., Qian, J., Blough, N. V. & Mopper, K. J. 2015 Insights into the photoproduction sites of hydroxyl radicals by dissolved organic matter in natural waters. *Environ. Sci. Technol. Lett.* **2** (12), 352–356.

Tang, X., Cui, Z., Bai, Y. & Su, R. 2020 Indirect photodegradation of sulfathiazole and sulfamerazine: Influence of the CDOM components and seawater factors (salinity, pH, nitrate and bicarbonate). *Sci. Total Environ.* **750**, 141762.

Vecchio, R. D. & Blough, N. V. 2004 On the origin of the optical properties of humic substances. *Environ. Sci. Technol.* **38** (14), 3885–3891.

Walse, S. S., Morgan, S. L., Kong, L. & Ferry, J. L. 2004 Role of dissolved organic matter, nitrate, and bicarbonate in the photolysis of aqueous fipronil. *Environ. Sci. Technol.* **38** (14), 3908–3915.

Wang, M., Xiang, X., Zuo, Y., Peng, J. & Gao, S. J. 2020 Singlet oxygen production abilities of oxidated aromatic compounds in natural water. *Chemosphere* **258**, 127308.

Wijnja, H., Pignatello, J. J. & Malekani, K. J. 2004 Formation of π–π complexes between phenanthrene and model π-acceptor humic subunits. *J. Environ. Qual.* **33**, 265–275.

Wu, X. & Shao, Y. X. 2017 Study of kinetics mechanism of PAHs photodegradation in solution. *Procedia Earth Planet. Sci.* **17**, 348–351.

Xia, X., Li, G., Yang, Z., Chen, Y. & Huang, G. H. 2009 Effects of fulvic acid concentration and origin on photodegradation of polycyclic aromatic hydrocarbons in aqueous solution: Importance of active oxygen. *Environ. Pollut.* **157** (4), 1352–1359.

Xue, S., Sun, J., Liu, Y., Zhang, Z., Lin, Y. & Liu, Q. 2019 Effect of dissolved organic matter fractions on photodegradation of phenanthrene in ice. *J. Hazard. Mater.* **361**, 30–36.

Zeng, C., Ji, Y., Zhou, L., Zhang, Y. & Yang, X. 2012 The role of dissolved organic matters in the aquatic photodegradation of atenolol. *J. Hazard. Mater.* **239–240**, 340–347.

Zhang, X., Su, H., Gao, P., Li, B., Feng, L. & Liu, Y. 2022 Effects and mechanisms of aged polystyrene microplastics on the photodegradation of sulfamethoxazole in water under simulated sunlight. *J. Hazard. Mater.* **433**, 128813.

Zhao, J., Zhou, Y., Li, C., Xie, Q., Chen, J. & Chen, G. 2020 Development of a quantitative structure-activity relationship model for mechanistic interpretation and quantum yield prediction of singlet oxygen generation from dissolved organic matter. *Sci. Total Environ.* **712**, 136450.

Zhu, D., Hyun, S., Pignatello, J. J. & Lee, L. 2004 Evidence for π-π electron donor-acceptor interactions between π-donor aromatic compounds and π-acceptor sites in soil organic matter through pH effects on sorption. *Environ. Sci. Technol.* **38**, 4361–4368.

Zularisam, A. W., Ismail, A. F., Salim, M. R., Sakinah, M. & Ozaki, H. 2007 The effects of natural organic matter (NOM) fractions on fouling characteristics and flux recovery of ultrafiltration membranes. *Desalination* **212** (1–3), 191–208.

First received 31 July 2023; accepted in revised form 27 October 2023. Available online 8 November 2023